Opt Quant Electron (2016) 48:143
DOI 10.1007/s11082-016-0416-2

Second harmonic generation and pulse shaping in positively and negatively spatially dispersive nanowaveguides: comparative analysis

Alexander K. Popov[1] · **Sergey A. Myslivets**[2,3]

Received: 26 July 2015 / Accepted: 16 January 2016 / Published online: 27 January 2016
© Springer Science+Business Media New York 2016

Abstract Comparative analysis of second harmonic generation in ordinary and backward-wave settings is presented. Extraordinary properties of frequency doubling nonlinear optical reflectivity and pulse shaping through phase matching of ordinary and backward electromagnetic waves in the nanowaveguides with mixed negative/positive spatial dispersion is demonstrated with numerical simulations.

Keywords Metamaterials · Nonlinear optics · Backward electromagnetic waves

1 Introduction

Metamaterials (MM) are artificially designed and engineered materials, which can have properties unattainable in nature. Usually, MM rely on advances in nanotechnology to build tiny metallic nanostructures smaller than the wavelength of light. These nanostructures modify the electromagnetic (EM) properties of MM, sometimes creating seemingly

This article is part of the Topical Collection on Optical Wave and Waveguide Theory and Numerical Modelling, OWTNM' 15.

Guest Edited by Arti Agrawal, B.M.A. Rahman, Tong Sun, Gregory Wurtz, Anibal Fernandez and James R. Taylor.

✉ Alexander K. Popov
popov@purdue.edu;
https://nanohub.org/groups/nlo/popov

Sergey A. Myslivets
sam@iph.krasn.ru

[1] Birck Nanotechnology Center, Purdue University, West Lafayette, IN 47907–2057, USA

[2] Institute of Physics of the Siberian Branch of the Russian Academy of Sciences , Krasnoyarsk, Russia 660036

[3] Siberian Federal University, 79 Svobodny pr., Krasnoyarsk, Russia 660041

impossible optical effects. Negative-index MM (NIMs) are the most intriguing EM materials that support backward EM waves (BEMW). Phase velocity and energy flux (group velocity) become *contra-directed* in NIMs. The appearance of BEMW is commonly associated with simultaneously negative electric permittivity ($\epsilon<0$) and magnetic permeability ($\mu<0$) at the corresponding frequency and, consequently, with negative refractive index $n = -\sqrt{\mu\epsilon}$. Counter-intuitive backwardness of EMW is in strict contrast with the electrodynamics of ordinary, positive-index materials. Extraordinary properties of nonlinear-optical frequency converting propagation processes has been predicted provided that one of the coupled EM waves falls in the negative-index frequency domain and propagates against the others (Shadrivov et al. 2006; Popov et al. 2006; Popov and Shalaev 2006a, b; Popov and Myslivets 2016). Among them are second harmonic generation (SHG) (Shadrivov et al. 2006; Popov et al. 2006; Popov and Shalaev 2006a; Popov and Myslivets 2016), optical parametric amplification (Popov and Shalaev 2006a, b) and frequency-shifted nonlinear reflectivity (Shadrivov et al. 2006; Popov et al. 2006; Popov and Shalaev 2006a, b; Popov and Myslivets 2011, 2016).

Current mainstream in fabricating bulk NIM slabs relies on engineering of LC nanocircuits—plasmonic mesoatoms with phase shifted, negative EM response. Extraordinary coherent, nonlinear optical, frequency converting propagation processes predicted in NIMs have been experimentally realized so far only in the microwave (Rose et al. 2011). A different paradigm which employs spatial dispersion (Lindell et al. 2001; Agranovich and Gartstein 2006; Agranovich et al. 2004; Nefedov and Tretyakov 2011) was proposed to realize outlined processes (Popov et al. 2012, 2013, 2014). Basic underlaying idea is nanoengineering negative spatial dispersion which would enable negative group velocity $v_{gr} = \partial\omega/\partial k<0$. Then energy flux, which is directed along the group velocity, appears directed *against* the wave vector. Such a property makes an analog of the effective negative refractive index. Basically, many hyperbolic MM may support backward-wave EM modes, see, e.g., Narimanov (2014), as well as specially designed waveguides (Mokhov et al. 2006; Salandrino and Christodoulides 2010). This opens new avenues for creation of backward-wave photonic devices with unparalleled functional properties.

As regards coherent *nonlinear-optical* propagation processes, *critically important* is to provide for *coexistence* of ordinary and backward coupled waves which frequencies and wave vectors satisfy to *energy and momentum* conservation law (*phase matching*). Particular metamaterial made of carbon nanotubes that can satisfy to the indicated requirements and enable such a possibility was proposed in Refs. Popov et al. (2012, 2013, 2014). Corresponding MM slabs can be viewed as the plasmonic nanowaveguides which support both ordinary EMWs with co-directed phase velocity and energy flux ($\partial\omega/\partial k > 0$) and extraordinary, BW modes with contra-directed phase and group velocities ($\partial\omega/\partial k<0$). Some of them exhibit spatial dispersion which changes from positive to negative in different wavelength intervals whereas the others predominantly maintain negative dispersion. Frequencies and gaps between the modes can be tailored by changing shapes, sizes and spacing of the MM nano-building blocks so that phase velocities for the modes matching the photon energy conservation law would become equal as their group velocities remain contra-directed. Basically, different materials and geometries can be utilized to control spatial dispersion and losses in such MM with variable spatial dispersion, see, e.g., Duncan et al. (2015).

Second harmonic generation (SHG) is the basic fundamental coherent (i.e., phase-dependent) nonlinear optical propagation process which finds many practically important application. Overall conversion efficiency is controlled by the intensity dependent local conversion rate and by the corresponding depletion of the fundamental beam. As shown in

Shadrivov et al. (2006), Popov et al. (2006), Popov and Shalaev (2006a, b), Popov and Myslivets (2011, 2016), such process exhibit unusual properties in the BW settings which are significantly different from both BW optical parametrical amplification and SHG in ordinary materials. This paper is to analyze such properties of SHG and fundamental differences between SHG in ordinary and backward-wave settings with focus on the pulse regime which is of particular practical interest.

2 Basic equations

As noted, the properties of SHG will be investigated for the cases where one of the coupled waves is ordinary and the other one is backward wave, in continuous-wave and pulse regimes, and compared with their ordinary counterparts. To achieve phase matching, phase velocities of the fundamental the SH waves must be co-directed. This means that in BW setting and pulse regime, the pulse of SH will propagate *against* the pulse of the fundamental radiation. Such extraordinary NLO coupling scheme dictates exotic properties of the *frequency-doubling ultracompact NLO mirror* under consideration, which are described below. One of our goals is to investigate the requirements for the magnitude of the metamaterial nonlinearity as well as for intensity of the control field(s) that would enable efficient functional properties of the indicated SHG mirror. Corresponding basic equations are as follows.

Electric and magnetic components of the waves and corresponding nonlinear polarizations are defined as

$$\{\mathcal{E},\mathcal{H}\}_j = \mathrm{Re}\{E,H\}_j \exp\{i(k_j z-\omega_j t)\}, \tag{1}$$

$$\{\mathcal{P},\mathcal{M}\}_j^{NL} = \mathrm{Re}\{P,M\}_j^{NL} \exp\{i(\widetilde{k}_j z-\omega_j t)\}, \tag{2}$$

$$\{P,M\}_1^{NL} = \chi^{(2)}_{e,m,1}\{E,H\}_2\{E,H\}_1^*, \tag{3}$$

$$\{P,M\}_2^{NL} = \chi^{(2)}_{e,m,2}\{E,H\}_1^2,\ 2\chi^{(2)}_{e,m,2} = \chi^{(2)}_{e,m,1}. \tag{4}$$

Equations for amplitudes E_j can be written as

$$s_2\frac{\partial E_2}{\partial z}+\frac{1}{v_2}\frac{\partial E_2}{\partial t} = -i\frac{k_2}{\epsilon_2}4\pi\chi^{(2)}_{e,2}E_1^2\exp(-i\Delta k z)-\frac{\alpha_2}{2}E_2, \tag{5}$$

$$s_1\frac{\partial E_1}{\partial z}+\frac{1}{v_1}\frac{\partial E_1}{\partial t} = -i\frac{k_1}{\epsilon_1}4\pi\chi^{(2)*}_{e,1}E_1^*E_2\exp(i\Delta k z)-\frac{\alpha_1}{2}E_1. \tag{6}$$

Here, $v_i > 0$ and $\alpha_{1,2}$ are group velocities and absorption indices at the corresponding frequencies, $\chi^{(2)}_{\mathrm{eff}} = \chi^{(2)}_{e,2} = \chi^{(2)}_{e,1}/2$ is effective nonlinear susceptibility, $\Delta k = k_2 - 2k_1$. Parameter $s_j = 1$ for ordinary, and $s_j = -1$ for backward wave. With account for $k^2 = n^2(\omega/c)^2$, $n_1 = s_1\sqrt{\epsilon_1\mu_1}$, $n_2 = s_2\sqrt{\epsilon_2\mu_2}$, we introduce amplitudes $e_j = \sqrt{|\epsilon_j|/k_j}E_j$, $a_j = e_i/e_{10}$, coupling parameters æ $= \sqrt{k_1k_2/|\epsilon_1\epsilon_2|}4\pi\chi^{(2)}_{\mathrm{eff}}$ and g = æE_{10}, loss and phase mismatch parameters $\widetilde{\alpha}_{1,2} = a_{1,2}L$ and $\Delta\widetilde{k} = \Delta k l$, slub thickness $d = L/l$, position $\xi = z/l$ and time instant $\tau = t/\Delta\tau$. It is assumed that $E_{j0} = E_j(z=0)$, $l = v_1\Delta\tau$ is the pump

pulse length, $\Delta\tau$ is duration of the input fundamental pulse. Quantities $|a_j|^2$ are proportional to the time dependent photon fluxes. Then Eqs. (5) and (6) are written as

$$s_2\frac{\partial a_2}{\partial\xi}+\frac{v_1}{v_2}\frac{\partial a_2}{\partial\tau}=-igla_1^2\exp\left(-i\Delta\widetilde{k}\xi\right)-\frac{\widetilde{\alpha}_2}{2d}a_2, \tag{7}$$

$$s_1\frac{\partial a_1}{\partial\xi}+\frac{\partial a_1}{\partial\tau}=-i2g^*la_1^*a_2\exp\left(i\Delta\widetilde{k}\xi\right)-\frac{\widetilde{\alpha}_1}{2d}a_1. \tag{8}$$

In the case of magnetic nonlinearity, $\chi_{\text{eff}}^{(2)}=\chi_{m,2}^{(2)}=\chi_{m,1}^{(2)}/2$, equations for the magnetic components of the fields $m_j=\sqrt{|\mu_j|/k_j}H_j$, $a_j=m_i/m_{10}$, take the form of (7) and (8) where coupling parameters are $\text{æ}=\sqrt{k_1k_2/|\mu_1\mu_2|}4\pi\chi_{\text{eff}}^{(2)}$ and $\text{g}=\text{æH}_{10}$. In both cases, $z_0=g^{-1}$ is characteristic medium length required for significant NLO energy conversion. Only most favorable case of the exact phase matching $\Delta k=0$ and loss-free medium ($\alpha_1=\alpha_2=0$) will be considered below.

3 Phase matched SHG of continuous wave in loss-free medium

For the case of $l\to\infty$, $\partial a_j/\partial\tau\to 0$ and $\widetilde{\alpha}_{1,2}=\Delta\widetilde{k}=0$, Eqs. (7) and (8) reduce to

$$s_2da_2/dz=-iga_1^2,\quad s_1da_1/dz=-i2g^*a_1^*a_2. \tag{9}$$

Manley–Rove equation (photon conservation law) derived from Eq. (9) is

$$s_2d|a_2|^2/dz+(1/2)s_1d|a_1|^2/dz=0. \tag{10}$$

3.1 SHG in ordinary NLO medium

For the case of ordinary waves $s_1=s_2=1$ and $a_{20}=0$ with account for $a_{10}=1$, one finds from Eq. (10) that

$$2|a_2|^2+|a_1|^2=1. \tag{11}$$

Solution to Eq. (9) is found as [Popov and Shalaev (2006a), Popov et al. (2006)]

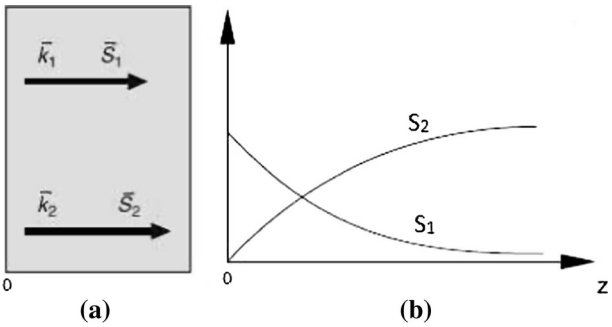

Fig. 1 Coupling geometry and energy fluxes in ordinary, positive index, materials

$$2|a_2|^2 = \tanh^2(\sqrt{2}gz), \quad |a_1|^2 = \mathrm{sech}^2(\sqrt{2}gz). \tag{12}$$

Figure 1a, b schematically show coupling geometry and energy fluxes $S_{2,1} \propto |a_{2,1}|^2$ across the ordinary, positive index material slab. According to Eqs. (11) and (12), *sum* of fluxes of photons $\hbar\omega_2$ and of the pairs of photons $\hbar\omega_1$ is conserved across the medium.

3.2 SHG in the nanowaveguide with mixed, negative at ω and positive at 2ω spatial dispersion

Figure 2a, b display coupling geometry and energy fluxes in the NLO slab in this case.

In the case of backward fundamental and ordinary SH waves, $s_1 = -1, s_2 = 1$, Eqs. (9) and (10) dictates fundamentally different behavior. Equation (10) predicts

$$|a_1|^2 - 2|a_2|^2 = |B|^2, \tag{13}$$

where $|B|^2$ is a constant which, however, depends on the slab thickness and on strength of the input fundamental field. Equations (9) reduce to

$$da_2/dz = -iga_1^2, \quad da_1/dz = i2g^* a_1^* a_2. \tag{14}$$

Besides the fact that the in this case the equations have different signs in the right sides, the boundary conditions for fundamental and SH waves must be applied to *opposite* edges of the slab of thickness L: $a_{10} = 1$, $a_{2L} = 0$. Indicated differences give rise to fundamental changes in the solution to the equations for the amplitudes and, consequently, to the properties of the SHG as a whole. Solution to Eq. (14) can be presented as [Popov and Shalaev (2006a), Popov et al. (2006)]

$$\sqrt{2}a_2 = B\tan[B\sqrt{2}g(L-z)], \tag{15}$$

$$a_1 = B\sec[B\sqrt{2}g(L-z)]. \tag{16}$$

As follows from (16), quantity B presents transmitted fundamental wave, $a_{1L} = B$. It is found from Eq. (16) at $z = 0$ as:

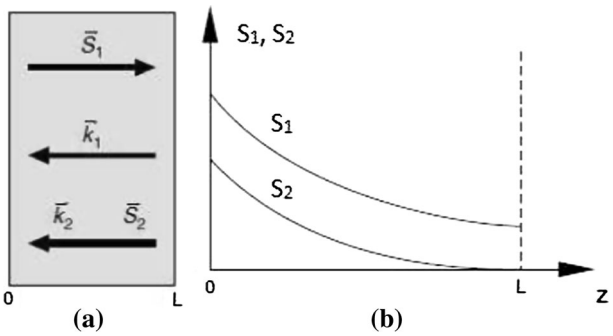

Fig. 2 Coupling geometry and energy fluxes in negative-index MM

$$B = \cos(B\sqrt{2}gL). \tag{17}$$

According to Eqs. (13) and (15)–(16), *difference* between the numbers of pairs of photons $\hbar\omega_1$ and the number of photons $\hbar\omega_2$ is conserved so that the number of photons $\hbar\omega_2$ at $z = L$ is always equal to zero. The later requirement controls whole process of BWSHG. Such a dependence is in strict contrast with SHG in ordinary NLO materials, where the SH flux may exceed the fundamental one in some area inside the slab. In the case of BWSHG, its energy flux is directed against the fundamental one towards the areas with higher intensity of the fundamental wave whereas remains lower everywhere inside the slab. As seen from Eq. (17), the gap between the two curves, $|B|^2$, decreases and, hence, the conversion efficiency grows with $gL = L/z_0 \to \infty$. Like in the preceding case, z_0 represents a characteristic medium length required for significant energy conversion to the SH. It shortens with growth of strength of the pump field.

3.3 Comparison of SHG for ordinary and backward fundamental waves

Figure 3a illustrates unparalleled properties of SH generation with backward wave as compared with its ordinary counterpart at similar other parameters for the particular example of $gL = 1$. As noted, the remarkable property is the fact that SH propagates against the fundamental wave and, therefore, metaslabs operates as a *frequency doubling metamirror* with reflectivity controlled by the fundamental wave. Further, the materials which support only ordinary waves and the MM that support both ordinary and backward

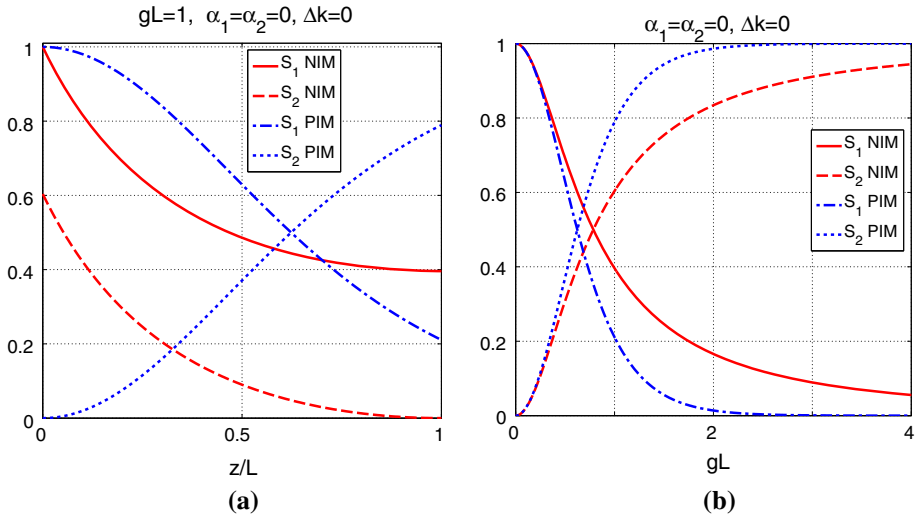

Fig. 3 Differences between SHG in ordinary and BW settings. **a** Energy fluxes across the slab for fundamental (the descending *dash-dotted blue line*) and SH (the ascending *dotted blue line*), both are ordinary waves in a positive-index (PIM) material; and for *backward-wave* fundamental (the descending *solid red line*) and ordinary-wave SH (the *descending dashed red line*) in a negative-index (NIM) slab. $gL = 1$. **b** Output transmitted fundamental (the descending *blue dash-dotted line*) and SH (the ascending *blue dotted line*) at $z = L$, both are ordinary waves in a PIM; and transmitted backward-wave fundamental (the descending *solid red line*) flux at $z = L$ and ordinary SH flux at $z = 0$ (the ascending *dashed red line*) in a NIM. (Color figure online)

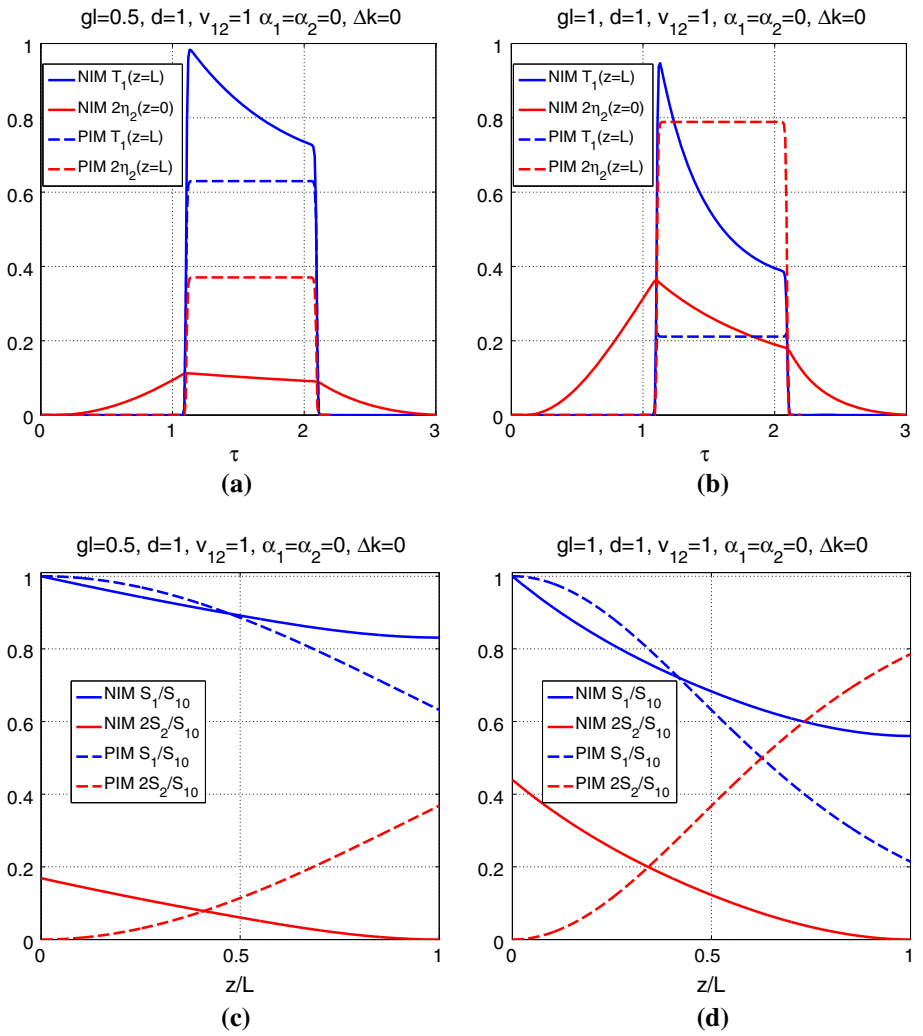

Fig. 4 Comparison of pulse shapes and energy conversion at SHG in ordinary (PIM) and backward-wave (NIM) settings in a loss-free MM. The length of input pulse at the fundamental frequency is equal to the metaslab thickness. **a**, **b** Input rectangular T_1 pulse shapes for the fundamental radiation; η_2—for SH. **c**, **d** Change of the pulse energy at the corresponding frequencies across the slab. Here, $d = L/l$, $S_1(z)$ and $S_{10} = S_1(z = 0)$ are fundamental pulse energy, $2S_2/S_{10}$ is energy (photon) conversion efficiency per pulse. (Color figure online)

waves will be referred to as PIM and NIM, accordingly. Figure 3b compares output intensity of the SH and transmitted fundamental wave in the BW and ordinary settings. Major important conclusion are as follows. It appears that the efficiency of SHG in the ordinary settings exceeds that in the NIM metaslab at equal other parameters. At that, propagation properties of SH in the BW settings appear fundamentally different which holds promise of extraordinary applications. Intensity of SH is less than that of the fundamental BW wave across the NIM slab, whereas it can exceed that in the vicinity of exit from PIM slab (Fig. 3a) Quantum conversion grows sharper with increase of intensity of

fundamental beam and higher conversion at lower intensities occurs in PIM as compared with NIM.

4 Comparison of ordinary and BW SHG in short-pulse regime

In this section, comparative analysis of SHG in the ordinary and BW settings will be done for the case where intensity of input fundamental wave varies in time and, therefore, SHG is described by the system of partial differential equations (7) and (8). The input pulse shape is chosen close to a rectangular form

$$F(\tau) = 0.5\left(\tanh\frac{\tau_0 + 1 - \tau}{\delta\tau} - \tanh\frac{\tau_0 - \tau}{\delta\tau}\right), \tag{18}$$

where $\delta\tau$ is the duration of the pulse front and tail, and τ_0 is the shift of the front relative to $t = 0$. Parameters $\delta\tau = 0.01$ and $\tau_0 = 0.1$ have been selected for numerical simulations. Absorption is neglected ($\alpha_1 = \alpha_2 = 0$). Phase velocities are equal $\Delta k = 0$. Group velocities are equal ($v_{12} = v_1/v_2 = 1$) and contra-directed. Strength of the input field is represented by the coupling parameter gl=l/z_0.

Unusual properties of SHG in NIMs in the pulsed regime stem from the fact that it occurs only inside the traveling pulse of fundamental radiation. Generation begins on its leading edge, grows towards its trailing edge, and then exits the fundamental pulse with no further changes. Since the fundamental pulse propagates across the slab, the duration of the SH pulse may occur significantly *longer* than that of the fundamental one. Depletion of the fundamental radiation along the pulse and the overall conversion efficiency depend not only on maximum intensity of the input pulse, on matching of phase and group velocities of the fundamental and second harmonic, but on the ratio of the fundamental pulse length and slab thickness. Such properties are in strict contrast with that of SHG in PIM as

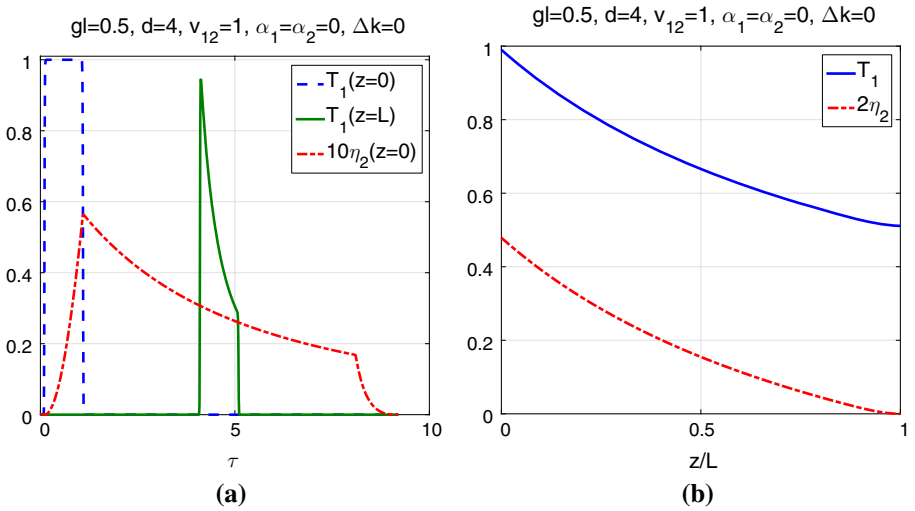

Fig. 5 Effect of the slab length. Here the slab length is increased in four times as compared with Fig. 4**a** and **b** at the same peak intensity. (Color figure online)

illustrated in Figs. 4 and 5. Shape of the input fundamental pulse is given by the function $T_1 = |a_1(\tau, z = 0)|^2/|a_{10}|^2$. The results of numerical simulations for the output fundamental pulse is given by $T_1 = |a_1(\tau, z = L)|^2/|a_{10}|^2$. Shape of the output pulse of SH at $z = 0$ is given by the function $\eta_2 = |a_2(\tau, z = 0)|^2/|a_{10}|^2$. Pulse energy is represented by the time integrated pulse areas S_j which varies across the slab. As seen from Fig. 4a, b, saturation is homogeneous across the pulse in PIM and shape of both fundamental and SH output pulses remain rectangular. On the contrary, shapes of the output fundamental and SH pulses in NIM are *different* and *change* with change of intensity of input fundamental pulse. Moreover, it appears that shapes of the output pulses varies with change of the slab length at unchanged other parameters as seen from comparison of Fig. 4a and Fig. 5a. Basic properties of pulse energy conversion across the NIM and PIM slabs qualitatively resemble those in continuous-wave regime (Figs. 4c, d and 5b). Its efficiency increases with increase of the slab length (cf. Figs. 4c, 5b). Figures 4c, d and 5b show an increase of the conversion efficiency with increase of intensity of the input pulse and of the slab thickness. It is followed by the shortening of the SH pulse.

Figures 4c, d and 5b satisfy to the conservation law in a loss-free metaslab: the number of annihilated pair of photons of fundamental radiation $(S_{10} - S_{1L})/2$ is equal to the number of output SH photons S_{20}. Figures 4a, b and 5a prove that shapes and width of fundamental and generated SH pulses as well as the energy conversion efficiency to the reflected pulses at doubled frequency can be controlled by changing intensity and ratio of the the input pulse length to the metamaterial thickness (parameter d).

5 Conclusions

Comparative analysis of SHG in ordinary and backward-wave settings in continuous and pulse regimes is presented. Backward-wave regime can be attributed to negative-index metamaterials or to the nanomaterials which possess spatial dispersion of opposite signs at fundamental at second harmonic frequencies. The latter make possible equal phase velocities of the coupled waves whereas their energy fluxes appear contra-directed. Such deliberately engineered nanolayers can be viewed as nanowaveguides. It is shown that properties of second harmonic generation in ordinary and backward-wave settings are fundamentally different. In the latter case, metaslab serves as microscopic frequency doubling nonlinear-optical mirror which properties can be all-optically controlled. In pulse regime, energy conversion property are qualitatively similar to those in continuous wave regime, whereas depend on the ratio of pulse length to the metaslab thickness. It is shown that width and shape of transmitted fundamental and generated second harmonic pulses can be controlled by changing intensity and width of input pulses as well as metamaterial thickness.

Acknowledgments This material is based upon work supported in part by the U. S. Army Research Laboratory and the U. S. Army Research Office under grant number W911NF-14-1-0619, by the National Science Foundation under grant number ECCS-1346547 and by the Russian Foundation for Basic Research under grant RFBR 15-02-03959A. We thank I. S. Nefedov, A. E. Boltasseva and V. M. Shalaev for inspiring inputs.

References

Agranovich, V.M., Gartstein, YuN: Spatial dispersion and negative refraction of light: Physics-Uspekhi (UFN). **176**, 10511068 (2006). In: Krowne C.M., Zhang, Y. (eds.) Physics of Negative Refraction. Springer, (2007)

Agranovich, V.M., Shen, Y.R., Baughman, R.H., Zakhidov, A.A.: Linear and nonlinear wave propagation in negative refraction metamaterials. Phys. Rev. B **69**, 165112 (2004)

Duncan, C., Perrel, L., Palomba, S., Lapine, M., Kuhlmey, B.T., de Sterke, C.M.: New avenues for phase matching in nonlinear hyperbolic metamaterials. Sci. Rep. **5**, 08983 (2015)

Lindell, I.V., Tretyakov, S.A., Nikoskinen, K.I., Ilvonen, S.: BW mediamedia with negative parameters, capable of supporting backward waves. Microw. Opt. Technol. Lett. **31**, 129–133 (2001). doi:10.1002/mop.1378

Mokhov, S., El-Ganainy, R., Christodoulides, D.N.: Power circulation via negative energy-flux wormholes in optical nanowaveguides. Opt. Express **14**, 3255–3262 (2006)

Narimanov, E.E.: Photonic hypercrystals. Phys. Rev. X **4**, 041014 (2014)

Nefedov, I., Tretyakov, S.: Ultrabroadband electromagnetically indefinite medium formed by aligned carbon nanotubes. Phys. Rev. B **84**, 113410–113414 (2011)

Popov, A.K., Myslivets, S.A.: Nonlinear-optical metamirror. Appl. Phys. A **103**, 725–729 (2011)

Popov, A.K., Myslivets, S.A.: Nonlinear-optical frequency-doubling meta-reflector: pulsed regime. Appl. Phys. A **122**(1), 1–6 (2016). doi:10.1007/s00339-015-9534-0

Popov, A.K., Shalaev, V.M.: Negative-index metamaterials: second harmonic generation, Manley–Rowe relations and parametric amplification. Appl. Phys. B Lasers Opt. **84**, 131–137 (2006a)

Popov, A.K., Shalaev, V.M.: Compensating losses in negative-index metamaterials by optical parametric amplification. Opt. Lett. **31**, 2169–2171 (2006b)

Popov, A.K., Shalaev, M.I., Myslivets, S.A., Slabko, V.V., Nefedov, I.S.: Enhancing coherent nonlinear-optical processes in nonmagnetic backward-wave materials. Appl. Phys. A **109**, 835–840 (2012). doi:10.1007/s00339-012-7390-8

Popov, A.K., Shalaev, M.I., Slabko, V.V., Myslivets, S.A., Nefedov, I.S.: Nonlinear backward-wave photonic metamaterials. Adv. Sci. Technol. **77**, 246–252 (2013). doi:10.4028/www.scientific.net/AST.77.246

Popov, A.K., Slabko, V.V., Shalaev, V.M.: Second harmonic generation in left-handed metamaterials. Laser Phys. Lett. **3**, 293–296 (2006)

Popov, A.K., Slabko, V.V., Shalaev, M.I., Nefedov, I.S., Myslivets, S.A.: Nonlinear optics with backward waves: extraordinary features, materials and applications. Solid State Phenomena **213**, 222–225 (2014). doi:10.4028/www.scientific.net/SSP.213.222

Rose, A., Huang, Da, Smith, D.R.: Controlling the second harmonic in a phase-matched negative-index metamaterial. Phys. Rev. Lett. **107**, 063902–063904 (2011)

Salandrino, A., Christodoulides, D.N.: Negative index Clarricoats–Waldron waveguides for terahertz and far infrared applications. Opt. Express **18**, 3626–3631 (2010)

Shadrivov, I.V., Zharov, A.A., Kivshar, YuS: Second-harmonic generation in nonlinear left-handed metamaterials. J. Opt. Soc. Am. B **23**, 529–534 (2006)